

Understanding fragility in supercooled Lennard-Jones mixtures.

I. Locally preferred structures

D. Coslovich* and G. Pastore†

*Dipartimento di Fisica Teorica, Università di Trieste – Strada Costiera 11, 34100 Trieste, Italy and
CNR-INFM Democritos National Simulation Center – Via Beirut 2-4, 34014 Trieste, Italy*

(Dated: October 24, 2018)

We reveal the existence of systematic variations of isobaric fragility in different supercooled Lennard-Jones binary mixtures by performing molecular dynamics simulations. The connection between fragility and local structures in the bulk is analyzed by means of a Voronoi construction. We find that clusters of particles belonging to locally preferred structures form slow, long-lived domains, whose spatial extension increases by decreasing temperature. As a general rule, a more rapid growth, upon supercooling, of such domains is associated to a more pronounced super-Arrhenius behavior, hence to a larger fragility.

PACS numbers: 61.43.Fs, 61.20.Lc, 64.70.Pf, 61.20.Ja

I. INTRODUCTION

What is the origin of super-Arrhenius behavior of transport coefficients and relaxation times in supercooled liquids? This is one of the long-standing, open questions regarding the physics of the glass-transition. Angell¹ introduced the notion of fragility to quantify the degree of super-Arrhenius behavior: generally speaking, the steeper the increase of relaxation times by decreasing temperature, the more fragile the glass-former. While relaxation times increase by several orders of magnitude on approaching the glass-transition, only mild variations in the average liquid structure are observed. Nevertheless, a subtle, deep link between microstructural order and dynamics is believed to exist.^{2,3,4} In particular, the emergence, upon supercooling, of slow domains, characterized by well-defined locally preferred structures,⁵ has been recently identified as a possible origin of super-Arrhenius behavior, both in numerical simulations^{6,7} and theoretical approaches.^{8,9,10} Despite some efforts in this direction, the microscopic foundations of such a connection have been explored only to a limited extent. In fact, the relation between fragility and local order has been explicitly investigated only for monoatomic systems,^{4,6,7} and operational schemes for a direct determination of locally preferred structures have not been tested yet for model supercooled liquids.^{11,12}

Understanding how fragility changes in different systems appears to be an even harder task. Experimentally, some interesting correlations have been proposed,^{13,14,15,16,17,18} but a sharp interpretation of these results is hindered by the complexity and the varying nature of intermolecular interactions. Numerical simulations, allowing fine-tuning of interaction parameters for a wide choice of potentials, are optimal tools for studying how the details of the interaction affect the be-

havior of supercooled liquids. Following this approach, some authors have recently investigated the connection between the features of the interaction potential and fragility.^{19,20,21,22} For instance, it has been shown that changing the power-law dependence of repulsion in a soft-sphere mixture leaves fragility invariant,¹⁹ while altering both repulsive and attractive parts of the Lennard-Jones potential can change the fragility of a supercooled mixture.²⁰ The role of intermolecular interactions should not, however, be overemphasized. Statistical mechanics theories of the glass-transition often use correlation functions or other coarse-grained information on the liquid properties as input, rather than the bare interaction potential. For instance, the most celebrated mode coupling theory²³ emphasizes the role of pair correlations, as described by the static structure factors. Providing correlations between fragility and properties such as local order, which may be used to characterize mesoscopic domains in supercooled liquids, would also be more helpful for understanding experimental trends.

In this paper, we investigate the connection between fragility and local order by performing Molecular Dynamics simulations of different supercooled Lennard-Jones mixtures. We consider a set of equimolar, additive mixtures with varying size ratio, together with some prototypical mixtures (Sec. II). Different from most numerical simulations on Lennard-Jones mixtures, we cool these systems at constant pressure (Sec. III). The isobaric fragilities obtained from relaxation times and diffusion coefficient show a systematic variation in additive mixtures upon varying size ratio (Sec. IV). Different fragility indexes are also found for two models^{24,25} that have often been employed in computational studies on the glass-transition. We rationalize these findings by analyzing the role of locally preferred structures, as identified by means of a Voronoi construction (Sec. V). We show that super-Arrhenius behavior of dynamical properties can be ascribed to a rapid growth, upon supercooling, of slow domains possessing distinct microstructural features. As a keynote, we find that the fragility of binary mixtures is correlated to the thermal rate of growth of such do-

*Electronic address: coslo@ts.infn.it

†Electronic address: pastore@ts.infn.it

mains: the more fragile the mixture, the more rapid the increase of the fraction of particles forming locally preferred structures.

II. MODEL BINARY MIXTURES

We have performed extensive Molecular Dynamics simulations for 13 binary Lennard-Jones mixtures. All models are composed of $N = 500$ classical particles enclosed in a cubic box with periodic boundary conditions. Particles interact via the Lennard-Jones potential

$$u_{\alpha\beta}(r) = 4\epsilon_{\alpha\beta} \left[\left(\frac{\sigma_{\alpha\beta}}{r} \right)^{12} - \left(\frac{\sigma_{\alpha\beta}}{r} \right)^6 \right] \quad (1)$$

where $\alpha, \beta = 1, 2$ are indexes of species. In our convention, particles of species 2 have a smaller diameter than those of species 1 ($\sigma_{22} < \sigma_{11}$), and we fix $\sigma_{11} = 1.0$ for all systems. Reduced units will be used in the following, assuming σ_{11} , ϵ_{11} and $\sqrt{m_1\sigma_{11}^2/\epsilon_{11}}$ as units of distance, energy and time respectively. We have employed the cut-off scheme of Stoddard and Ford,²⁶ which ensures continuity up to the first derivative of $u_{\alpha\beta}(r)$ at the cutoff radius $r_c = 2.5$.

The interaction parameters of the mixtures considered in this work are shown in Table I. These models are characterized by a varying degree of non-additivity in the composition rule for the cross interaction and by different values of size ratio $\lambda = \sigma_{22}/\sigma_{11}$. Deviations from Lorentz-Berthelot composition rules can be quantified using

$$\eta = \frac{\sigma_{12}}{(\sigma_{11} + \sigma_{22})/2} \quad \xi = \frac{\epsilon_{12}}{\sqrt{\epsilon_{11}\epsilon_{22}}} \quad (2)$$

We will now proceed to a brief presentation of the relevant features of these force fields.

BMLJ – Binary Mixture of Lennard-Jones particles

This is the classic mixture of Kob and Andersen,²⁴ which has been used extensively as a model supercooled liquid. It is characterized by a significant asymmetry in the interaction parameters, both in the interaction diameters and in the energy scales of the two species. Furthermore, cross interactions are strongly non-additive ($\eta = 0.85$, $\xi = 2.1$). The number concentration of large particles is fixed at $x_1 = 0.8$, as in the original work.

Ni₃₃Y₆₇ – Lennard-Jones model for Ni₃₃Y₆₇ alloy

The parametrization of this mixture has been introduced by Della Valle *et al.*²⁷ to provide a realistic description of the structural features of binary amorphous alloys of Ni and Y atoms. The cross-interaction diameter is non-additive ($\eta = 0.91$), as in the case of BMLJ, but

TABLE I: Parameters of Lennard-Jones potentials for binary mixtures. Also shown are the masses m_1 and m_2 of the two species and the concentration x_1 of particles of species 1. In the case of additive mixtures AMLJ- λ , the following values of size ratio λ have been used: 0.60, 0.64, 0.70, 0.73, 0.76, 0.82, 0.88, 0.92, 0.96, 1.00.

	BMLJ	Ni ₃₃ Y ₆₇	WAHN	AMLJ- λ
σ_{11}	1.0	1.0	1.0	1.0
σ_{12}	0.8	0.7727	0.916	$(\lambda + 1)/2$
σ_{22}	0.88	0.6957	0.833	λ
ϵ_{11}	1.0	1.0	1.0	1.0
ϵ_{12}	1.5	1.0	1.0	1.0
ϵ_{22}	0.5	1.0	1.0	1.0
m_1	1.0	1.0	1.0	1.0
m_2	1.0	1.0	0.5	1.0
x_1	0.8	0.67	0.5	0.5

a single energy scale is present. The masses of the two chemical species are equal. The number concentration $x_1 = 0.67$ allows deep supercooling of the mixture.

WAHN – Additive mixture of Wahnström

Introduced by Wahnström,²⁵ this equimolar mixture is actually the Lennard-Jones version of the supercooled soft-sphere model used in the early simulations of Bernu *et al.*²⁸ It has been employed several times in the literature as a model glass-former. The interaction parameters are additive and characterized by a moderate size asymmetry ($\lambda = 0.837$). Note that the mass ratio is $m_2/m_1 = 0.5$.

AMLJ- λ – Additive Mixture of Lennard-Jones particles

This is a set of equimolar additive mixtures. The masses of the two species are equal $m_1 = m_2 = 1.0$ and the size ratio λ is allowed to vary, keeping σ_{11} fixed at 1.0. Recently, Lennard-Jones clusters of this type has been investigated.²⁹ Ten different values of λ have been used in the range $0.60 \leq \lambda \leq 1.0$. Note that AMLJ-0.837 would be the same as the WAHN mixture, if not for the the different mass ratio.

III. QUENCHING PROTOCOLS AND SIMULATION DETAILS

Numerical simulations of model supercooled liquids are usually performed at constant density. Recently, some attention has been drawn to density effects^{30,31} and to the role of pressure.^{32,33} Nonetheless, numerical studies of supercooled Lennard-Jones mixtures along isobaric

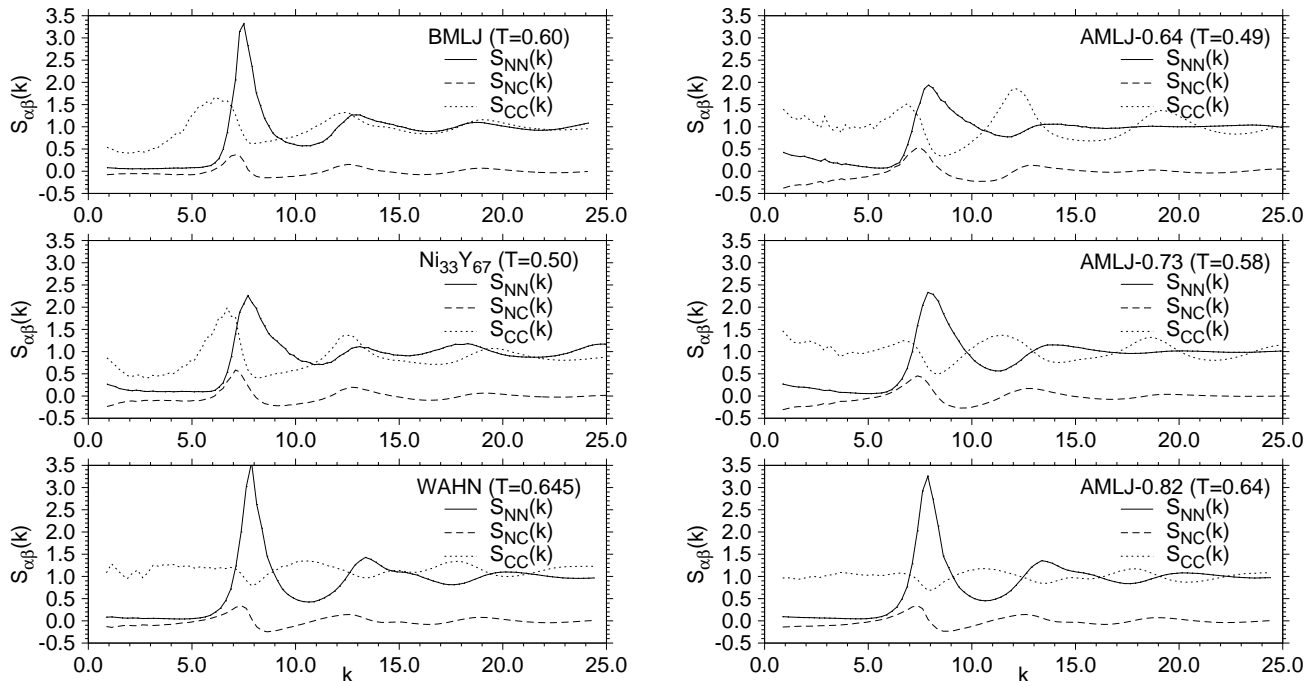


FIG. 1: Bathia-Thornton structure factors in the deeply supercooled regime. Number-number (solid lines), number-concentration (dashed lines) and concentration-concentration (dotted lines) structure factors are shown. The concentration-concentration structure factor has been normalized to one by plotting $S_{CC}(k)/(x_1x_2)$. Data are shown at the lowest equilibrated temperature for each given system. Note that all structure factors are finite in the limit $k \rightarrow 0$ and that the first sharp peak of $S_{NN}(k)$ around $k_0 \approx 8$ is roughly system independent.

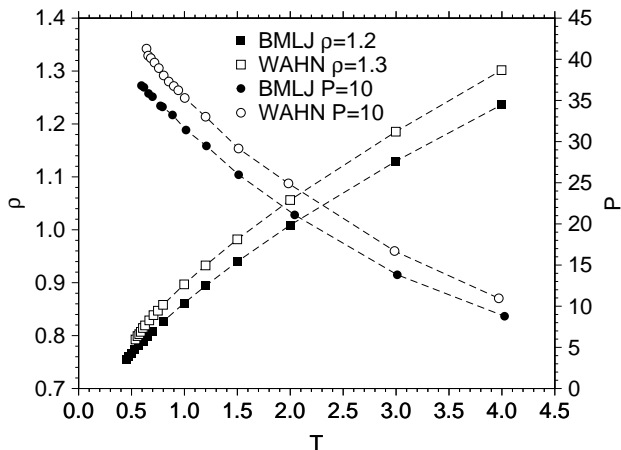


FIG. 2: Temperature dependence of density $\rho(T)$ along isobaric quenches at $P = 10$ (left axis, circles) and of pressure $P(T)$ in isochoric quenches (right axis, squares). Data are shown for BMLJ (filled symbols) and WAHN (open symbols). Isochoric quenches were performed at $\rho = 1.2$ for BMLJ and $\rho = 1.3$ for WAHN.

quenches have seldom been performed. In our case, following cooling paths at a common, constant pressure provides a simple mean to perform a homogeneous compar-

ison of different mixtures. Moreover, this approach is closer to the one usually employed in experimental conditions, where most comparisons of supercooled liquids are performed at constant (atmospheric) pressure. Whereas some minor differences between isochoric and isobaric quenches can be observed, and will be highlighted in the following, we remark that the main conclusions of this work are independent of the choice of the quenching protocol.

Isobaric quenches were performed by coupling the system to both Berendsen thermostat and barostat during the equilibration phase. In most cases, we employed the standard Velocity-Verlet algorithm for production runs. In order to achieve better control on temperature in the deeply supercooled regime, we also performed a few production runs using the Nosé-Poincaré thermostat.^{34,35} For the system size and temperatures in consideration, simulations in different ensembles provide consistent results, as far as average dynamical and thermodynamical properties are concerned. Isochoric quenches were performed in a similar way, using the Berendsen thermostat only during equilibration. The timestep δt of both Velocity-Verlet and Nosé-Poincaré integrators was varied from 0.002 at high temperature to 0.006 in the supercooled regime. The time constant for the Berendsen thermostat³⁶ was $t_T = \delta t/0.1$, while the coupling constant for Berendsen barostat³⁶ was 10^3 in reduced units.

The inertia parameter of the Nosé-Poincaré thermostat was set to $Q = 5$. Thanks to the symplectic nature of the integrators and to the smooth cutoff employed, no significant drift in the relevant conserved Hamiltonian is observed in either kind of simulation used for production runs, even for very long runs (up to 2.5×10^7 steps at the lowest equilibrated temperatures).

Beside checking the stability of mean potential energy and pressure during the production phase, we adjusted the total simulation times in order to achieve similar values of total root mean square displacement for all state points and for all mixtures. Typical values of total root mean square displacement for large particles are always larger than $4\sigma_{11}$. To check the reliability of our results, we also tried both faster and slower cooling rates, and performed some thermal histories by reheating deeply supercooled samples. In the case of AMLJ- λ mixtures, we found that they could be safely supercooled for values of size ratio λ between 0.60 and 0.84. In the case $\lambda = 0.88$, in fact, some early signs of crystallization were found in our sample. A part from this case, no sign of phase separation or crystallization was detected looking at the time evolution of thermodynamic and structural properties. The Bathia-Thornton³⁷ number-number, number-concentration and concentration-concentration structure factors for a selection of mixtures are shown in Fig. 1 at the lowest equilibrated temperatures.

In the following, we will mostly consider isobaric quenches performed at a reduced pressure $P = 10$. Reference data for BMLJ are available along this isobar,³² so that we could check the reliability of both dynamical and thermodynamical properties obtained in our simulations. In the case of BMLJ, we performed a few isobaric quenches over a wider range of pressure ($P = 5, 10, 20, 50$) to investigate the pressure dependence of isobaric fragility. Isochoric quenches have been performed for BMLJ and WAHN mixtures, fixing the density at $\rho = 1.2$ and $\rho = 1.3$ respectively. These values of ρ are equal to the ones used in the original papers.^{24,25} In Fig. 2 we show the temperature dependence of density (at constant pressure) and pressure (at constant density) for BMLJ and WAHN. Note that the range of pressure investigated for BMLJ ($5 \leq P \leq 50$) is consistent with the variation of pressure for this system along the isochore $\rho = 1.2$.

IV. FRAGILITY

The fragility of a glass-former quantifies how rapid the change of dynamical properties is upon supercooling. We will focus on dynamical quantities that can be computed with good statistical accuracy in numerical simulations, namely relaxation times for the decay of density fluctuations and diffusion coefficients.

For the definition of relaxation times we will consider

the self part of the intermediate scattering function

$$F_s^\alpha(k, t) = \frac{1}{N_\alpha} \sum_{i=1}^{N_\alpha} \langle \exp \{ i\mathbf{k} \cdot [\mathbf{r}_i(t + t_0) - \mathbf{r}_i(t_0)] \} \rangle \quad (3)$$

where $\alpha = 1, 2$ is an index of species and $\langle \rangle$ indicates an average over time origins t_0 . Relaxation times τ_α for species α are defined by the condition $F_s^\alpha(k^*, \tau_\alpha) = 1/e$, where k^* corresponds to the position of the first peak in the number-number structure factor (see Fig. 1). The value of k^* is roughly system- and temperature independent for the mixtures in consideration, and close to $k \approx 8$. In the following, we will focus on the temperature dependence of $\tau \equiv \tau_1$, but similar trends are observed when considering the small particles.

The difficulty of providing an unbiased, global description of the temperature dependence of transport coefficients and relaxation times by fitting the experimental data has been particularly stressed by Kivelson *et al.*³⁸ Care must be taken when the definition of fragility itself relies on a specific functional form, or when the latter is used for extrapolations outside the accessible range of temperature. We thus seek functional forms that are reliable over a large range of temperature and require the range for fitting to be well-specified and physically motivated. For describing the temperature dependence of relaxation times, we start with the well-known Vogel-Fulcher-Tammann (VFT) law and write it in the form³⁹

$$\tau(T) = \tau_\infty \exp \left[\frac{1}{K(T/T_0 - 1)} \right] \quad (4)$$

The material-dependent parameter K quantifies the fragility of the glass-former under consideration. The larger is K , the steeper is the increase of $\tau(T)$ upon supercooling. Equation (4) provides a fairly good description of relaxation times in the deeply supercooled regime, but is inaccurate at high temperature.³⁸ In the normal liquid regime, in fact, relaxation times have a mild temperature dependence, which is well described by the Arrhenius law. The existence of a crossover between these two regimes around some temperature T_{onset} , accompanied by several qualitative changes in the properties of the liquid, is well established in the literature⁵⁸. It seems thus sensible to use the following global functional form

$$\tau(T) = \begin{cases} \tau_\infty \exp [E_\infty/T] & T > T^* \\ \tau'_\infty \exp \left[\frac{1}{K(T/T_0 - 1)} \right] & T < T^* \end{cases} \quad (5)$$

where

$$\tau'_\infty = \tau_\infty \exp \left[E_\infty/T^* - \frac{1}{K(T^*/T_0 - 1)} \right] \quad (6)$$

as a generalized VFT law. This functional form is continuous at the crossover temperature T^* and provides a fragility index K with analogous physical meaning to that in Eq. (4). To fit our simulation data to Eq. (4),

TABLE II: Fitted parameters for relaxation times $\tau(T)$ of large particles according to the generalized Vogel-Fulcher-Tammann given by Eq. (5), and for total diffusion coefficient $D(T)$ according to Eq. (7). The reference temperature T_r and the onset temperature T_{onset} are described in the text.

	P	T_{onset}	T_r	Relaxation times			Diffusion coefficient		
				τ_∞	E_∞	T_0	K	T_0	K
BMLJ	5.0	0.75	0.464	0.0931(3)	1.99(1)	0.392(3)	0.43(2)	0.361(6)	0.37(2)
BMLJ	10.0	0.95	0.574	0.0815(5)	2.61(1)	0.479(2)	0.40(1)	0.457(3)	0.41(1)
BMLJ	20.0	1.20	0.765	0.067(1)	3.71(9)	0.63(1)	0.40(5)	0.60(1)	0.42(3)
BMLJ	50.0	1.80	1.248	0.0481(9)	6.60(7)	1.03(1)	0.38(3)	1.01(1)	0.46(2)
WAHN	10.0	0.90	0.623	0.0825(4)	2.33(1)	0.573(4)	0.94(6)	0.523(6)	0.70(4)
WAHN	20.0	1.20	0.825	0.0670(6)	3.38(3)	0.752(5)	0.84(5)	0.697(9)	0.68(4)
Ni ₃₃ Y ₆₇	10.0	0.90	0.489	0.0777(7)	2.53(2)	0.391(3)	0.31(1)	0.379(4)	0.37(1)
AMLJ-0.60	10.0	0.85	0.451	0.076(1)	2.43(3)	0.341(5)	0.24(1)	0.319(4)	0.29(1)
AMLJ-0.64	10.0	0.90	0.474	0.07691(3)	2.444(1)	0.381(4)	0.32(1)	0.356(4)	0.36(1)
AMLJ-0.70	10.0	0.90	0.514	0.0811(1)	2.359(4)	0.440(5)	0.48(3)	0.417(7)	0.51(4)
AMLJ-0.73	10.0	0.90	0.560	0.0785(7)	2.48(2)	0.502(4)	0.71(4)	0.466(6)	0.62(4)
AMLJ-0.76	10.0	0.90	0.601	0.0790(9)	2.49(3)	0.554(4)	1.01(9)	0.519(7)	0.84(7)
AMLJ-0.82	10.0	0.95	0.636	0.0803(5)	2.53(1)	0.591(6)	1.1(1)	0.53(1)	0.76(7)
	ρ	T_{onset}	T_r	τ_∞	E_∞	T_0	K	T_0	K
BMLJ	1.2	1.00	0.422	0.110(2)	2.69(2)	0.331(3)	0.31(1)	0.328(2)	0.426(9)
WAHN	1.3	1.05	0.522	0.097(1)	2.73(2)	0.447(5)	0.50(4)	0.426(2)	0.64(1)

we proceed similarly to Kivelson *et al.*³⁸ First we fit the relaxation times to the Arrhenius law $\tau_\infty \exp(E_\infty/T)$ in the range $T > T_{onset}$ and then we use τ_∞ and E_∞ as fixed parameters in a global fit to Eq. (5). In this way, a good overall fit is obtained for relaxation times. Note that T^* is considered as a fitting parameter, but the main conclusions of this section will not be altered by fixing $T^* = T_{onset}$.

The Angell plots of relaxation times in Fig. 3 and Fig. 4 constitute the starting point of our discussion. For their construction we have used a reference temperature T_r , akin to the glass transition temperature T_g , at which $\tau(T_r) = 4 \times 10^4$. Such a value of $\tau(T_r)$ is close to the one used by Bordat *et al.*²⁰ in a study of modified Lennard-Jones mixtures. For each mixture, the value of the reference temperature T_r , which we have extrapolated using Eq. (5), is only slightly below the lowest equilibrated temperature.

In Fig. 3 we consider the set of additive, equimolar mixtures AMLJ- λ along isobaric quenches at $P = 10$. The size ratio λ is varied in the range $0.60 \leq \lambda \leq 0.82$. A strong, systematic variation is apparent upon varying λ : the mixture becomes more fragile as λ increases, i.e. as the size asymmetry between the two species is reduced. Recently, a similar influence of size ratio on fragility has been observed in modified BMLJ mixtures.²² The trend of variation of fragility is confirmed by our fitting procedure, whose outcome is summarized in Table II. The dependence of the isobaric fragility index K on λ , shown in the inset of Fig. 3, also suggests the existence of a saturation of fragility around $\lambda = 0.80$. This feature will be further discussed in Sec. V, in connection with icosahedral ordering.

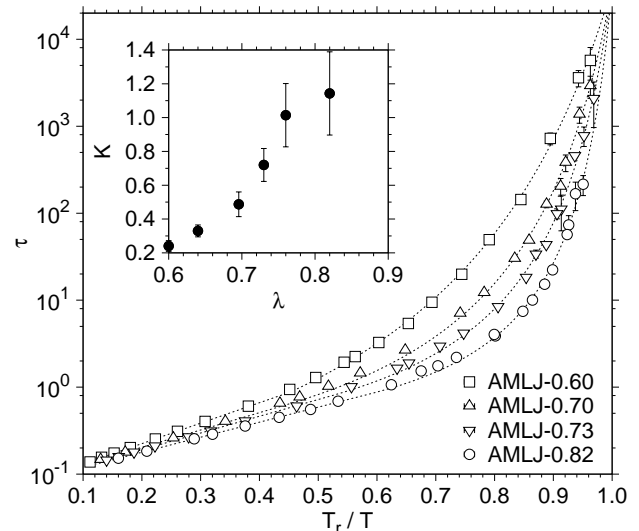


FIG. 3: Angell plot of relaxation times of large particles τ for a selection of AMLJ- λ mixtures. Results are shown for $\lambda = 0.60, 0.70, 0.73, 0.82$ along the isobar $P = 10$. The reference temperature T_r is described in the text. The inset shows the isobaric fragility index K obtained from generalized VFT equation (see Eq. (5)) against size ratio λ .

dral ordering.

Figure 4 shows the temperature dependence of relaxation times for the two well-studied glass-formers BMLJ and WAHN, both cooled isobarically at $P = 10$. These mixtures have been used extensively for numerical inves-

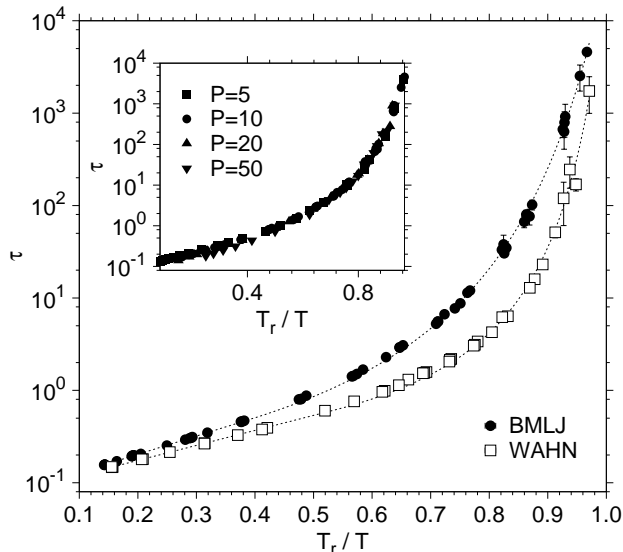


FIG. 4: Angell plot of relaxation times of large particles τ for BMLJ (black circles) and WAHN mixture (white circles) along isobaric quenches at $P = 10$. The inset shows results at $P = 5, 10, 20, 50$ for BMLJ.

tigations of the glass-transition, but a direct comparison has never appeared in the literature. We find that WAHN is appreciably more fragile than BMLJ, independent of quenching protocols and system size⁵⁹. The enhanced fragility of WAHN is not surprising since this mixture is, a part from a different mass ratio, an AMLJ- λ mixture with $\lambda = 0.837$. We found that such difference in mass ratio is irrelevant to the dynamical properties in consideration. Thus, WAHN can be considered as the end-point of a series of supercooled mixtures with increasingly large fragility.

Does isobaric fragility itself depend on pressure? This question has received much attention in the last years, in particular within the experimental community.^{40,41,42,43,44} A tentative answer can be given for BMLJ, for which we performed isobaric quenches in the range $5 \leq P \leq 50$. By looking at the inset of Fig. 4, we can see that relaxation times obtained along different isobars collapse on a master curve by scaling T with the corresponding T_r . Numerical values of isobaric fragility K , obtained from Eq. (5) along different isobars, are also very close to each other (see Table II). Thus, our results indicate that the pressure dependence of isobaric fragility of Lennard-Jones mixtures might be mild or even negligible for moderate variations of P . For a given system, we also find that the isochoric fragility is slightly smaller than the corresponding isobaric fragility, in agreement with experimental observations.⁴²

As another dynamical indicator we consider the the total diffusion coefficient $D = x_1 D_1 + x_2 D_2$, given by the usual Einstein relation. The temperature dependence of D can be described quite satisfactorily over the entire

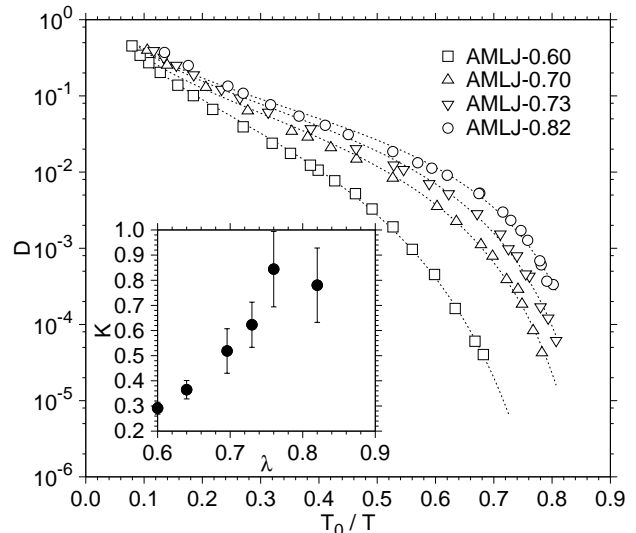


FIG. 5: Angell plot of total diffusion coefficient D for a selection of AMLJ- λ mixtures. Results are shown for $\lambda = 0.60, 0.70, 0.73, 0.82$ along the isobar $P = 10$. The reference temperature T_0 is obtained from fit to Eq. (7). The inset shows the isobaric fragility index K obtained from Eq. (7) against size ratio λ .

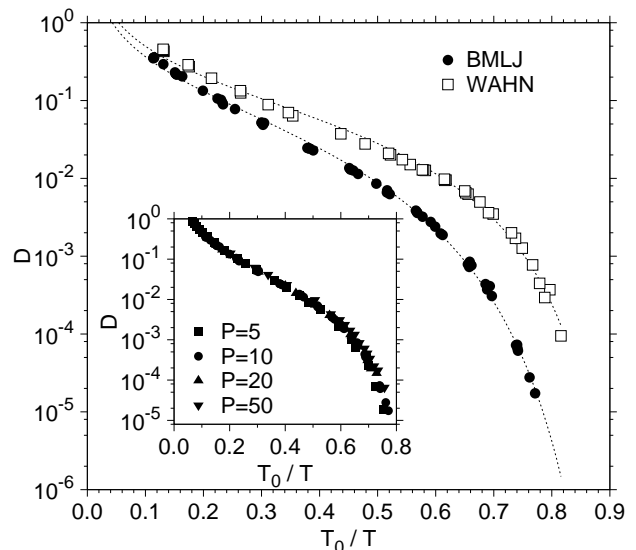


FIG. 6: Angell plot of total diffusion coefficient D for BMLJ (black circles) and WAHN mixture (white circles) along isobaric quenches at $P = 10$. The inset shows results at $P = 5, 10, 20, 50$ for BMLJ.

temperature range by a modified VFT law⁴⁵

$$D(T) = D_0 T \exp \left[-\frac{1}{K(T/T_0 - 1)} \right] \quad (7)$$

Again, the parameter K in Eq. (7) provides a measure of fragility. Angell plots for the diffusion coefficient are

shown in Figs. 5 and 6, and results of fits to Eq. (7) are collected in Table II. Regarding the variation of fragility in our models, results obtained for the diffusion coefficient confirm the analysis based on relaxation times. Note that, by considering the temperature dependence of both $\tau \equiv \tau_1$ and D , we account for a possible dependence of fragility on chemical species and k -vector. Thus, the following trends appear to be rather robust: (i) The increase of fragility with size ratio λ in AMLJ- λ mixtures. (ii) The less fragile behavior of BMLJ compared to WAHN. (iii) The independence of isobaric fragility on pressure in BMLJ.

V. LOCALLY PREFERRED STRUCTURES

The growth of long-lived, slow domains, characterized by well-defined structural features, has been discussed recently in connection to super-Arrhenius behavior of dynamical properties of supercooled liquids.^{4,6,7,8} In this section, we will follow a similar approach by analyzing the properties of local order in the Lennard-Jones mixtures introduced in Sec. II. We will highlight the existence of different, well-defined local geometries in these systems and show how their properties are related to the variations of fragility.

For this kind of analysis we have employed a Voronoi construction.⁴⁶ Each particle in the system is the center of a Voronoi polyhedron, which is constructed by intersection of planes orthogonal to all segments connecting the central particle to the other ones. Planes are drawn at a fraction $f_{\alpha\beta}$ of these segments, where α is the species of the central particle and β is the species of the other particle. We have used the recipe $f_{\alpha\beta} = \sigma_{\alpha\alpha}/(\sigma_{\alpha\alpha} + \sigma_{\beta\beta})$,²⁷ but the main conclusions of this section will not be altered when considering the more intuitive choice, $f_{\alpha\beta} = 1/2$. The sequence (n_3, n_4, \dots) , where n_k is the number of faces of the polyhedron having k vertices, provides a detailed description of the local geometry around a given particle. All zero values behind the maximum number of vertices of a polyhedron are ignored. We have applied this kind of analysis to both instantaneous configurations, sampled along Molecular Dynamics trajectories, and to local minima of the potential energy, obtained by conjugate-gradients minimizations. Between 200 and 2000 independent configurations have been analyzed for each state point. We found that it is easier to characterize local order in the Lennard-Jones mixtures considered in this work by taking “the point of view” of small particles. Well-defined geometries appear, in fact, most frequently around small particles, while no recognizable local order is apparent around large particles. In the following, we will thus concentrate our attention on the properties of Voronoi polyhedra centered around small particles.

Such a Voronoi construction will provide an indication of what are the locally preferred structures^{8,11} of our model supercooled liquids. In the rest, we will use

TABLE III: Most frequent Voronoi polyhedra around small particles. The percentage is computed with respect to the number of small particles in the system. Also shown is the average number of neighbors of species 1 (n_1) and 2 (n_2). Results refer to local minima along the isobar $P = 10$ and are shown for $T = 2.0$ and slightly above the reference temperature T_r , i.e. for the lowest equilibrated temperature.

	$T = 2.00$				$T \approx T_r$			
	%	Signature	n_1	n_2	%	Signature	n_1	n_2
AMLJ-0.64	12.0	(0,2,8,1)	7	4	13.9	(0,2,8,1)	7	4
	7.3	(0,2,8,2)	6	6	9.3	(0,2,8,2)	7	5
	7.1	(0,2,8)	7	3	8.3	(0,2,8)	7	3
	5.8	(0,3,6,3)	7	5	6.7	(0,3,6,3)	7	5
AMLJ-0.70	11.8	(0,2,8,1)	7	4	12.1	(0,0,12)	5	7
	10.2	(0,2,8,2)	7	5	11.8	(0,2,8,2)	7	5
	5.9	(0,3,6,3)	7	5	11.6	(0,2,8,1)	7	4
	5.0	(0,3,6,4)	7	6	6.7	(0,3,6,4)	7	6
AMLJ-0.82	14.3	(0,0,12)	6	6	29.1	(0,0,12)	6	6
	10.9	(0,2,8,2)	7	5	10.8	(0,2,8,2)	7	5
	7.3	(0,3,6,4)	7	6	8.1	(0,1,10,2)	7	6
	6.7	(0,1,10,2)	7	6	6.9	(0,3,6,4)	8	5
WAHN	14.6	(0,0,12)	6	6	31.4	(0,0,12)	6	6
	10.7	(0,2,8,2)	7	5	10.1	(0,2,8,2)	7	5
	7.5	(0,3,6,4)	7	6	8.6	(0,1,10,2)	7	6
	7.1	(0,1,10,2)	7	6	7.1	(0,3,6,4)	8	5
BMLJ	13.7	(0,2,8)	9	1	18.6	(0,2,8)	10	0
	7.4	(1,2,5,2)	9	1	7.3	(1,2,5,3)	10	1
	7.3	(0,3,6)	9	0	6.1	(1,2,5,2)	9	1
	5.4	(0,3,6,1)	9	1	6.0	(0,3,6)	9	0
NiY	8.5	(0,3,6)	7	2	14.0	(0,3,6)	8	1
	6.6	(0,3,6,1)	8	2	9.3	(0,3,6,1)	8	2
	5.2	(0,4,4,3)	8	3	8.6	(0,2,8)	9	1
	5.1	(0,2,8)	8	2	6.1	(1,2,5,2)	9	1

an effective, purely geometric definition of locally preferred structures, as the ones corresponding to the most frequent polyhedra found in our Voronoi construction. Determining unambiguously the *origin* of the preference for a given local structure in the bulk will require a significant additional effort, since, in general, such preference will depend in a non-trivial way on the environment surrounding a given local structure and may be triggered by factors other than energetic stability. For instance, packing effects can play an important role in stabilizing a local structure. Moreover, in the case of binary mixtures, compositional freedom further increases the complexity of such analysis. Taking into account the effect of the liquid environment around a local structure at a mean-field level, and identifying the appropriate “local free energy” to be minimized, remains an open issue of current research.^{11,12} Here, we tackle these issues by using a purely geometric definition of locally preferred structures, which has the further advantage of being available even when

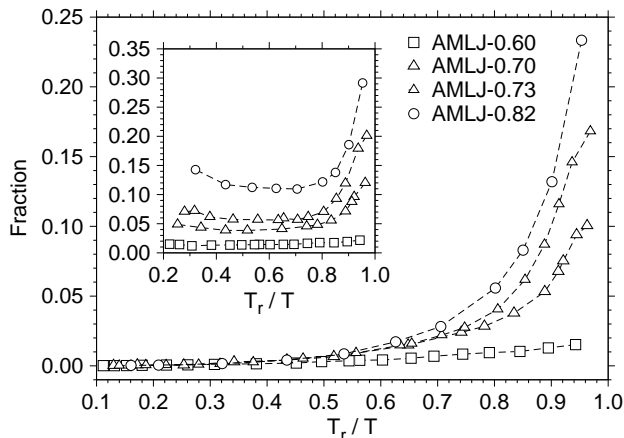


FIG. 7: Temperature dependence of the fraction of small particles at the center of (0,0,12)-polyhedra in AMLJ- λ for selected values of λ . Results are shown for instantaneous configurations (main plot) and local minima (inset) along isobaric quenches at $P = 10$.

energetic criteria will fail, e.g. for hard-spheres.

Let us first focus on equimolar, additive mixtures AMLJ- λ . One of the most relevant structural features of these mixtures is the existence of a varying degree of icosahedral ordering. Icosahedral coordination has a sharp signature in the Voronoi construction, being associated to (0,0,12)-polyhedra, i.e. 12 pentagonal faces. The temperature dependence of the fraction of icosahedra for different AMLJ- λ mixtures, shown in Fig. 7, displays a striking correlation with the variation of fragility. In fact, the increase of icosahedral ordering upon supercooling is more rapid and more pronounced as λ increases, i.e. as the fragility of the mixture increases⁶⁰. To our knowledge, this is the first time that such a relationship is established in supercooled binary mixtures. Previous numerical studies have focused, in fact, on the connection between icosahedral ordering and super-Arrhenius behavior in monoatomic liquids.^{6,7} The theoretical interpretation of our results is by no means trivial. On the one hand, the variation of fragility with icosahedral ordering may be understood within the frustration-limited domains theory⁸ in terms of a more rapid stabilization, upon supercooling, of locally preferred structures—in the present case, icosahedra—. We will further discuss this point below. On the other hand, the trend we find in our simulations and shown in Fig. 7 appears to be at variance with the results of a recent phenomenological model.^{9,10} Further clarifications on the relevance of this theoretical approach to our simulated systems are required.

To have a better feeling of how icosahedral ordering is triggered by size ratio, we show, in Fig. 8, the fraction of (0,0,12)-polyhedra in local minima as a function of λ . Results are shown along the isotherm $T = 2.0$ and for $T \approx T_r$, i.e. at the lowest temperatures that

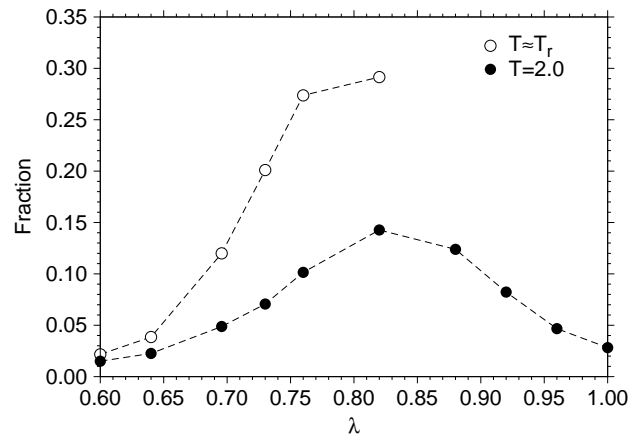


FIG. 8: Variation of icosahedral ordering with size ratio in additive mixtures AMLJ- λ . The fraction of small particles at the center of (0,0,12)-polyhedra in local minima is shown as a function of size ratio λ , at $T = 2.0$ (black circles) and at the lowest equilibrated temperatures (open circles).

could be accessed in equilibrium condition. Depending on temperature, a different range of λ is considered. In the deeply supercooled regime ($T \approx T_r$) only mixtures with $0.60 \leq \lambda \leq 0.84$ could be equilibrated (see Sec. III). For variation of λ in this range, icosahedral ordering increases with size ratio, in a way which strongly resembles the increase of fragility index K with λ , reported in Sec. IV. At high temperature ($T = 2.0$) the full range $0.60 \leq \lambda \leq 1.00$ can be accessed and our data reveal the existence of a maximum of icosahedral ordering around $\lambda \approx 0.82$. This feature might provide a simple explanation to the existence of a saturation of fragility around $\lambda = 0.80$ reported in Sec. IV. Interestingly, the results obtained from local minima at high temperature show that the variation of icosahedral ordering with size ratio, which is apparent in the deeply supercooled regime, is already encoded in the liquid inherent structure.⁴⁷

Such a pattern of variation of icosahedral ordering with size ratio is strikingly similar to that observed in models of bidisperse Cu glasses⁴⁸ and in the realistic models of metallic glasses developed by Hausleitner and Hafner.^{49,50} This suggests that the increase of icosahedral ordering with size ratio, and its consequent correlation with fragility, might be a general feature of binary systems with additive, or nearly additive, spherical interactions⁶¹. Furthermore, the onset of crystallization for $\lambda \gtrsim 0.88$ could be simply explained, in this kind of systems, by the decrease of icosahedral coordination and by a larger occurrence of (0,3,6,4)-polyhedra and (0,4,4,6)-polyhedra, which are typical of FCC crystals.⁵¹ We found, in fact, that the fraction of FCC-related polyhedra in the normal liquid regime increases as $\lambda \rightarrow 1$. A similar behavior has been explicitly demonstrated for the bidisperse Cu model by means of a Honeycutt-Andersen construction.

We can now generalize the connection between fragility

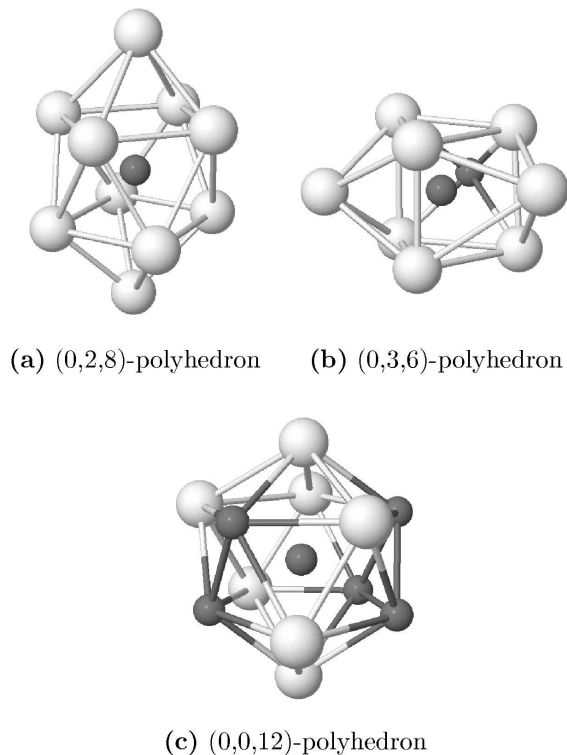


FIG. 9: Examples of locally preferred structures found in local minima of supercooled Lennard-Jones mixtures. Small and large particles are shown as dark and pale spheres respectively. (a) (0,2,8)-polyhedron (twisted bicapped square prism) in BMLJ. This is the most frequent chemical coordination, incidentally one or two small particles can form the cap. (b) (0,3,6)-polyhedron (capped trigonal prism) in $\text{Ni}_{33}\text{Y}_{67}$. In this case, one of the caps is often formed by a small particle. (c) (0,0,12)-polyhedron (icosahedron) in WAHN. On average, the coordination around the central particle is equimolar.

and locally preferred structures by analyzing systems possessing favored geometries different from icosahedra. Such opportunity is provided by non-additive mixtures, such as BMLJ and $\text{Ni}_{33}\text{Y}_{67}$. In the case of $\text{Ni}_{33}\text{Y}_{67}$, in fact, icosahedral ordering has been shown to be strongly frustrated.²⁷ Non-additivity of the interaction potential favors the formation of trigonal prismatic structures,²⁷ similar to those found in the crystalline phases of NiY alloys. This is confirmed by our analysis, which shows (see Table III) that the most frequent Voronoi polyhedron around small particles in $\text{Ni}_{33}\text{Y}_{67}$ is the (0,3,6)-polyhedron, corresponding to capped trigonal prismatic structures. In the case of BMLJ, we find that the (0,2,8)-polyhedron has the largest occurrence around small particles both at high and low temperature (see Table III). This polyhedron corresponds to twisted bicapped square prisms, mostly formed by neighboring large particles. The preference for twisted prismatic structures in BMLJ has also been highlighted in studies on the coordination polyhedra in the liquid,⁵² and on the stability of isolated clusters.⁵³ As a working hypothesis, we iden-

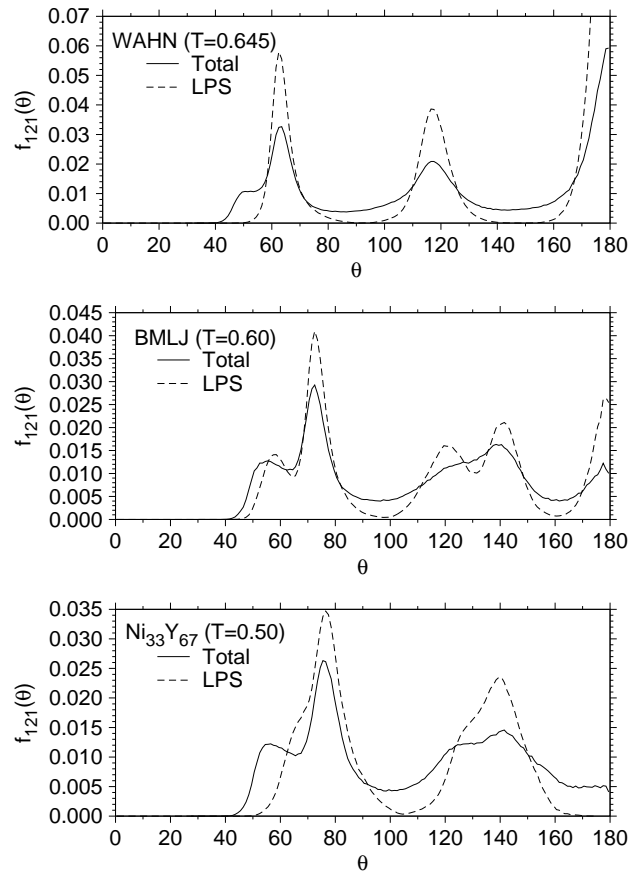


FIG. 10: Bond-angle distributions around small particles for WAHN (upper plot), BMLJ (middle plot) and $\text{Ni}_{33}\text{Y}_{67}$ (lower plot). The bond-angle distribution $f_{121}(\theta)$ is shown as solid line. Also shown is the bond-angle distribution $f_{121}(\theta)$ restricted to small particles which are at the center of the locally preferred structure of the system, as given by Fig. 9. Data refer to the lowest equilibrated temperature of each given system. The sharp peaks in the $f_{121}(\theta)$ distributions filtered for locally preferred structures reflect the ideal angles of the corresponding geometry.

tify the geometries associated to (0,3,6)-polyhedra and (0,2,8)-polyhedra as the locally preferred structures of $\text{Ni}_{33}\text{Y}_{67}$ and BMLJ, respectively. These two non-additive mixtures can be effectively contrasted to WAHN, which displays a strong icosahedral ordering upon supercooling.

In Fig. 9 we show three highly symmetric configurations corresponding to locally preferred structures, found in local minima of WAHN, BMLJ and $\text{Ni}_{33}\text{Y}_{67}$. Notice that the structures shown in the figure are among the most symmetric in their own class of Voronoi polyhedra. Support to our definition of locally preferred structures is given by the analysis of angular distributions. To this aim, we compute the bond-angle distribution functions $f_{\alpha\beta\gamma}(\theta)$ around particles of species α , where β and γ are the species of the neighboring particles. Particles sharing a face in the Voronoi construction are considered as neighbors. In Fig. 10 we focus on the bond-angle distri-

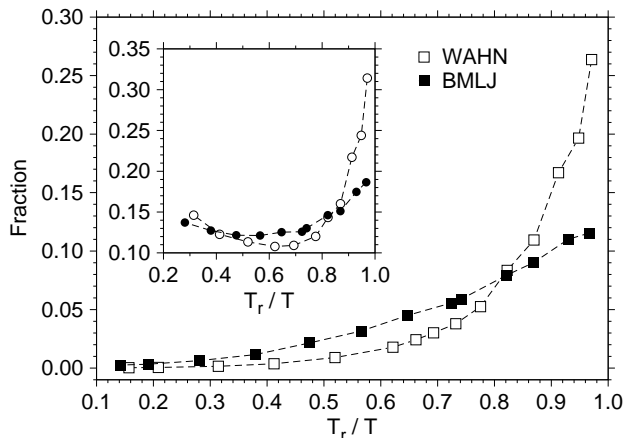
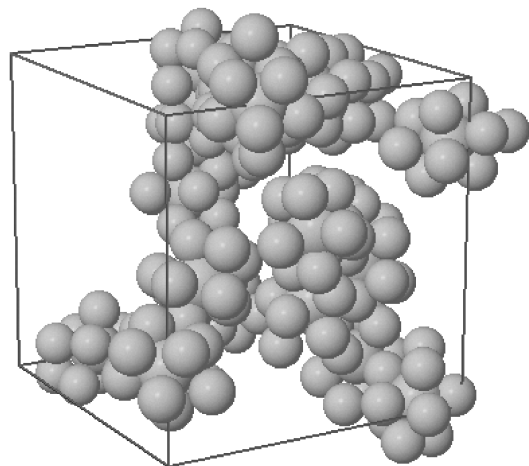


FIG. 11: Temperature dependence of the fraction of small particles at the center of selected Voronoi polyhedra in instantaneous configurations (main plot) and local minima (inset). The fraction of (0,2,8)-polyhedra in BMLJ (white symbols) and (0,0,12)-polyhedra in WAHN mixture (black symbols) are shown along isobaric quenches at $P = 10$. Data for $\text{Ni}_{33}\text{Y}_{67}$ are close to those for BMLJ, but are not shown for clarity.

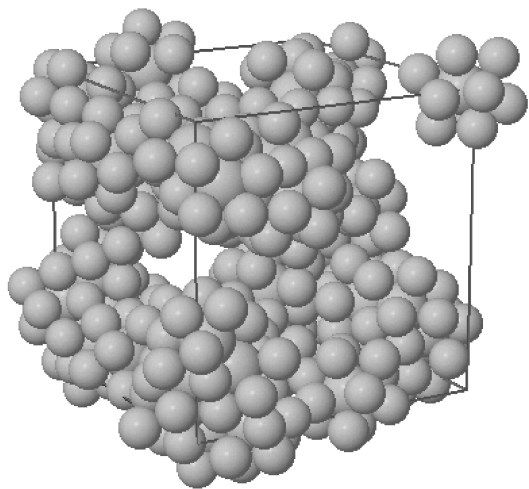
bution $f_{121}(\theta)$ for central small particles and neighboring large particles in WAHN, BMLJ and $\text{Ni}_{33}\text{Y}_{67}$. We compare the total $f_{121}(\theta)$ to the one restricted to small particles being the center of the typical Voronoi polyhedron of the mixture. A strong resemblance is observed between the average environment around small particles in the bulk and the local geometries of Voronoi polyhedra corresponding to our putative locally preferred structures.

As it can be seen from Fig. 11, the thermal rate of growth of the fraction of particles forming locally preferred structures is again correlated to the fragility of the model. In fact, the fraction of icosahedra in WAHN increases rapidly by decreasing temperature, whereas the growth of prismatic structures, typical of BMLJ and $\text{Ni}_{33}\text{Y}_{67}$, is rather mild. The most frequent Voronoi polyhedra of all these mixtures are not homogeneously spread in the system. They tend to form growing domains as the temperature decreases. This feature is exemplified by the two snapshots in Fig. 12, where we show the typical extension of domains formed by locally preferred structures in local minima, for deeply supercooled BMLJ and WAHN mixtures. Similar extended domains formed by interlocking icosahedra have been found in the supercooled regime of Dzugutov liquids.^{6,7}

To assess the statistical relevance of the presence of such domains, we analyze the distribution $P(N)$ of clusters composed by N neighboring particles forming locally preferred structures. Our identification of domains is as follows. For each given configuration, we partition the particles into three classes: (i) c -particles, which are the center of a locally preferred structure; (ii) n -particles, which are neighbors to some other c -particle, but are not themselves centers of a locally preferred structure; (iii)



(a) BMLJ ($P = 10$, $T = 0.60$)



(b) WAHN ($P = 10$, $T = 0.645$)

FIG. 12: Domains formed by locally preferred structures in local minima at the lowest equilibrated temperature at $P = 10$ (WAHN: $T = 0.645$. BMLJ: $T = 0.60$). Particles forming (a) (0,2,8)-polyhedra in BMLJ and (b) (0,0,12)-polyhedra in WAHN are shown as spheres of the same radius, irrespectively of chemical species.

o -particles, which are neither c -particles nor n -particles, i.e. they are outside the domains formed by locally preferred structures. Particles sharing a face in the Voronoi construction are then considered as neighbors. Using the partitioning scheme above, we identify domains as clusters composed by neighboring c - and n - particles. The distribution $P(N)$ is shown in Fig. 13 for instantaneous configurations of BMLJ and WAHN at different state points. By decreasing temperature, a clear tendency of forming larger clusters is observed in both systems. In the WAHN mixture we find that, around T_r , there is almost always a large cluster formed by icosahedra percolating in the simulation box, beside some smaller ones. This feature is reflected in the bimodal distribution of

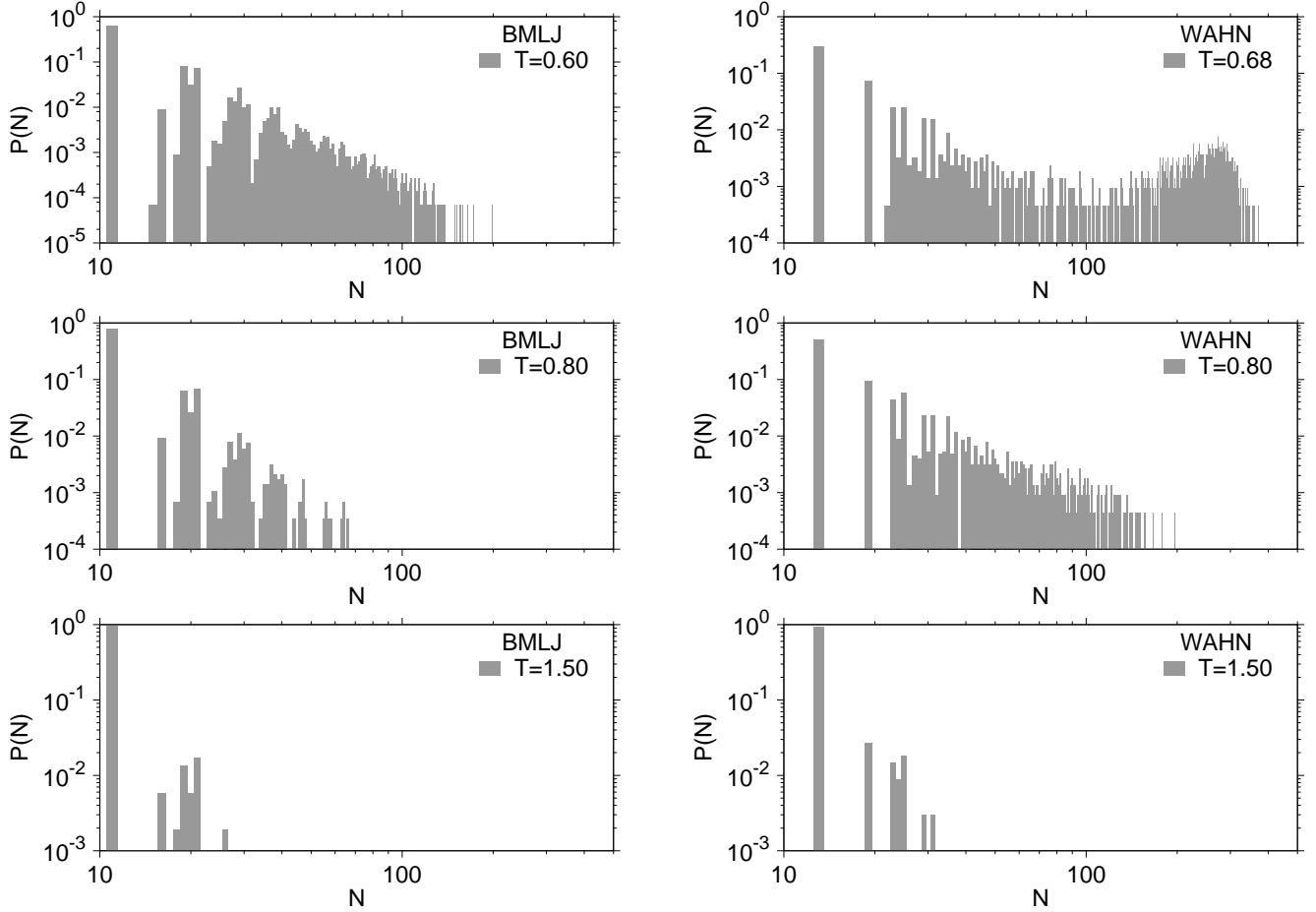


FIG. 13: Distribution $P(N)$ of the size N of domains formed by locally preferred structures in BMLJ (left plots) and WAHN (right plots) at different T . Results refer to isobaric quenches at $P = 10$.

$P(N)$ for WAHN at low temperature. On the other hand, as expected from the analysis of Fig. 11, the growth of domains in BMLJ appears to be more limited.

Such domains are expected to provide an efficient mechanism of slowing down in supercooled liquids.⁶ To address this issue, we evaluate the self intermediate scattering function for small particles [see Eq. (3)], according to their role in the locally preferred structure at time $t = t_0$. At each time origin t_0 , we partition the *small* particles into *c*-, *n*-, and *o*-particles, as described above. The correlation functions $F_s^c(k, t)$, $F_s^n(k, t)$, and $F_s^o(k, t)$ are then obtained by performing the average over time origins in Eq. (3) using only *c*-, *n*-, or *o*-particles respectively. Relaxation times τ_c , τ_n , and τ_o are defined as in Sec. IV. The ratio τ_c/τ_o provides a simple measure of the slowness of particles inside domains formed by a particular locally preferred structure. The temperature dependence of τ_c/τ_o is shown in Fig. 14 for various mixtures at $P = 10$. The value of τ_c/τ_o tends to 1 at high temperature in all systems and increases more markedly by decreasing temperature, as the fragility of the system increases. Around T_r , we find that relaxation times

within icosahedral domains differ by roughly an order of magnitude from those outside, whereas prismatic structures in non-additive mixtures develop a more modest separation of time scales.

The dynamical impact of locally preferred structures is assisted, at low temperature, by an increased lifetime of such slow domains. To address this point we proceeded similarly to Donati *et al.*,⁵⁴ introducing a single-particle function $\nu_i(t)$ that equals 1 if particle i is at the center of a given Voronoi polyhedron, and 0 if not. Restricting our attention to small particles, we computed the autocorrelation function⁵⁴

$$\sigma(t) = \sum_{i=1}^{N_2} \langle \nu_i(t) \nu_i(0) \rangle - \frac{n_p^2}{N_2} \quad (8)$$

where $n_p = \sum_{i=1}^{N_2} \langle \nu_i(0) \nu_i(0) \rangle$ is the average number of small particles at the center of a given polyhedron. We estimated the lifetime τ_p of a polyhedron from the condition $\sigma(\tau_p) = \sigma(0)/e$. Independent of the polyhedron under consideration, the normalized autocorrelation function $\sigma(t)/\sigma(0)$ falls rapidly to zero in the normal liquid

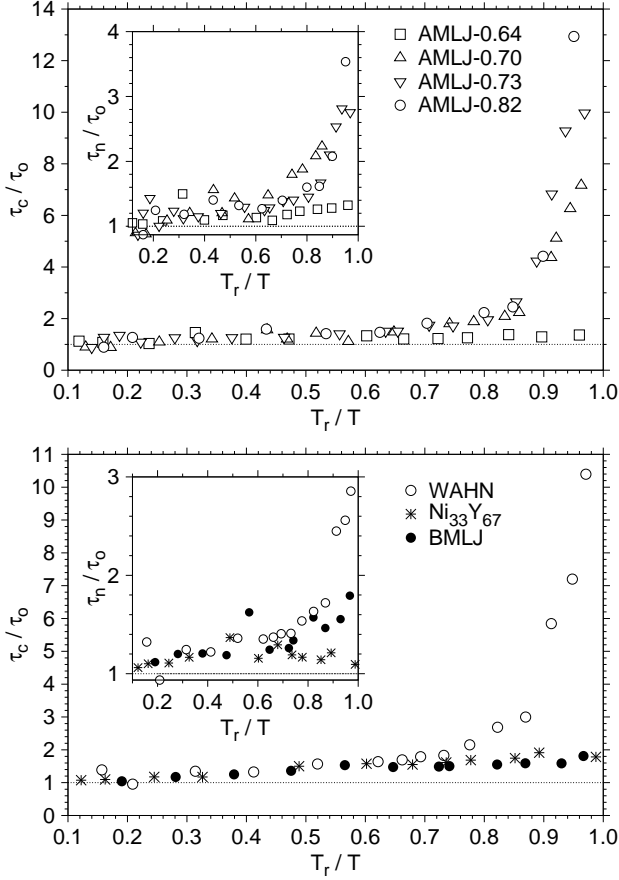


FIG. 14: Dynamical impact of locally preferred structures, as identified by the temperature dependence of the ratio τ_c/τ_0 (main plot) and τ_n/τ_0 (insets) at $P = 10$. See text for definition of τ_c , τ_n , and τ_0 . Upper plot: AMLJ- λ mixtures for $\lambda = 0.60, 0.70, 0.73, 0.82$. Lower plot: BMLJ (filled circles), WAHN (open circles) and Ni₃₃Y₆₇ (stars). The dotted line drawn at 1 indicates the high temperature limit.

regime. As the temperature is lowered, polyhedra corresponding to locally preferred structures become more long-lived than the others, as expected. Around T_r , we find that $\sigma(t)/\sigma(0)$ for locally preferred structures decays to zero within the time scale given by the decay of $F_s^2(k^*, t)$. In Table IV, we report the lifetimes τ_p of some frequent polyhedra found at the lowest equilibrated temperatures for WAHN, BMLJ, and Ni₃₃Y₆₇. In WAHN and BMLJ, the lifetime of polyhedra corresponding to locally preferred structures is around an order of magnitude larger than those of other geometries. Interestingly, in the case of Ni₃₃Y₆₇, we find that some less frequent polyhedra, such as (0,2,8)-polyhedra, have a lifetime comparable to that of our putative locally preferred structures, suggesting the existence of competing structures. We also find that icosahedra tend to have a longer lifetime, relative to the typical structural relaxation times, than prismatic structures.

The relation between fragility and local order, which is

TABLE IV: Lifetime τ_p of most frequent Voronoi polyhedra around small particles. Results are obtained from local minima at the lowest equilibrated temperatures ($T \approx T_r$). Also shown is the ratio τ_p/τ_2 , where τ_2 is the relaxation time obtained from the condition $F_s^2(k^*, \tau) = 1/e$.

	$T \approx T_r$		
	Signature	τ_p	τ_p/τ_2
WAHN	(0,0,12)	2000	1.6
	(0,1,10,2)	90	0.1
	(0,2,8,2)	60	0.0
	(0,3,6,4)	60	0.0
BMLJ	(0,2,8)	800	0.4
	(0,3,6)	200	0.1
	(1,2,5,3)	70	0.0
	(1,2,5,2)	40	0.0
Ni ₃₃ Y ₆₇	(0,2,8)	2500	0.5
	(0,3,6)	1600	0.3
	(0,3,6,1)	1300	0.3
	(1,2,5,2)	90	0.0

apparent from our simulation data, fits rather well into the scenario of the frustration-limited domains theory.⁸ According to this approach, glass-formation arises from the competition of a tendency to form mesoscopic, stable domains, characterized by locally preferred structures, and a mechanism of frustration, which prevents these domains from tiling three dimensional space. Fragility turns out to be proportional to the energetic stability of such domains and inversely proportional to the strength of frustration. At present, the roles of stability and frustration cannot be clearly disentangled. Nevertheless, the following considerations, based on the present work, are possible and we hope they could serve as guidelines for further theoretical modeling or investigations: (i) In the case of additive mixtures, within the explored range of size ratio, icosahedral ordering seems to be the most prominent structural feature. Results obtained for isolated Lennard-Jones clusters²⁹ suggest that the maximum of icosahedral ordering around $\lambda \approx 0.84$ might be related to an enhanced energetic stability of equimolar icosahedra, i.e. icosahedra with the same number of large and small neighbors. Formation of more stable icosahedral structures would, in turn, explain the increase of fragility with size ratio. A more detailed study of larger clusters in the bulk, forming extended regions of icosahedral coordination,^{6,7} would probably be required to further clarify this point. (ii) It should be realized that frustration in different systems may be of different origin. Icosahedral ordering, while being frustrated from tiling three-dimensional space for geometrical reasons, allows the growth of relatively large domains, when compared to prismatic structures observed in non-additive Lennard-Jones mixtures. In non-additive alloys different competing locally preferred structures and mismatch in

stoichiometry may further increase frustration.

VI. CONCLUSIONS

In this work, we have provided a comparative study of different supercooled Lennard-Jones mixtures by quenching the systems at constant pressure. The models analyzed include the well-studied mixtures BMLJ²⁴ and WAHN,²⁵ a set of equimolar, additive mixtures with varying size ratio, and a model meant to give a realistic structural description of the Ni₃₃Y₆₇ alloy.²⁷ These systems display a varying degree of fragility, which has been rationalized in terms of the properties of some relevant locally preferred structures.

Local order has been characterized using a Voronoi construction. Employing an effective definition of the locally preferred structure of a liquid, as the geometry corresponding to the most frequent Voronoi polyhedra, we have shown that fragility is related, in the mixtures considered in this work, to the rapid growth with temperature of slow, stable domains characterized by the locally preferred structure of the mixture, generalizing previous observations on monoatomic bulk systems.^{6,7} Such a growth with temperature is more rapid, the more fragile the mixture.

Analyzing the set of AMLJ- λ mixtures, we found that the size ratio λ controls the formation of icosahedral ordering in the bulk. Extended regions of icosahedral coordination are more rapidly formed upon supercooling of additive mixtures with moderate size asymmetry. This, in turn, leads to a more pronounced super-Arrhenius behavior. These results might also be representative of a wider class of mixtures with additive, non-directional interactions, since icosahedral ordering has been found to

display a similar trend of variation with size ratio in models of bidisperse Cu glasses.⁴⁸ On the other hand, non-additive mixtures, such as BMLJ and Ni₃₃Y₆₇, favor the formation of prismatic structures. The growth, upon supercooling, of these structures is milder compared to that of icosahedra in additive mixtures. Consequently, non-additive mixtures display a less fragile behavior, which might be due to the presence of stronger frustration mechanisms. From such discussion of our data, it is thus tempting to relate fragility to the thermal rate of growth of locally preferred structures, whatever their type may be.

In the light of the frustration-limited domains theory,⁸ fragility should originate from the interplay between stability of domains formed by locally favored geometries and frustration. Our results indicate that further studies are needed to assess the relative role of these two factors in supercooled mixtures. Deeper investigations on the link between fragility and local order, either by study of isolated clusters²⁹ or by direct determination of locally preferred structures in the bulk^{11,12} or by confocal microscopy technique,⁵⁵ will certainly be rewarding.

Acknowledgments

The authors would like to thank R. G. Della Valle for making available to us his efficient program for Voronoi analysis. Computational resources for the present work have been partly obtained through a grant from “Iniziativa Trasversale di Calcolo Parallelo” of the Italian *CNR-Istituto Nazionale per la Fisica della Materia* (CNR-INFM) and partly within the agreement between the University of Trieste and the Consorzio Interuniversitario CINECA (Italy).

-
- ¹ C. A. Angell, *J. Phys. Chem. Solids* **49**, 863 (1988).
² M. D. Ediger, *Annu. Rev. Phys. Chem.* **51**, 99 (2000).
³ A. Widmer-Cooper and P. Harrowell, *J. Phys.: Condens. Matter* **17**, S4025 (2005).
⁴ H. Shintani and H. Tanaka, *Nature Physics* **2**, 200 (2006).
⁵ F. C. Frank, *Proc. R. Soc. A* **215**, 42 (1952).
⁶ M. Dzugutov, S. I. Simdyankin, and F. H. M. Zetterling, *Phys. Rev. Lett.* **89**, 195701 (2002).
⁷ J. P. K. Doye, D. J. Wales, F. H. M. Zetterling, and M. Dzugutov, *J. Chem. Phys.* **118**, 2792 (2003).
⁸ G. Tarjus, S. A. Kivelson, Z. Nussinov, and P. Viot, *J. Phys.: Condens. Matter* **17**, R1182 (2005).
⁹ H. Tanaka, *J. Non-Cryst. Solids* **351**, 3371 (2005).
¹⁰ H. Tanaka, *J. Non-Cryst. Solids* **351**, 3385 (2005).
¹¹ S. Mossa and G. Tarjus, *J. Chem. Phys.* **119**, 8069 (2003).
¹² S. Mossa and G. Tarjus, *J. Non-Cryst. Solids* **352**, 4847 (2006).
¹³ K. Ito, C. T. Moynihan, and C. A. Angell, *Nature (London)* **398**, 492 (1999).
¹⁴ K. L. Ngai, *J. Non-Cryst. Solids* **275**, 7 (2000).
¹⁵ T. Scopigno, G. Ruocco, F. Sette, and G. Monaco, *Science* **302**, 849 (2003).
¹⁶ V. N. Novikov, Y. Ding, and A. P. Sokolov, *Phys. Rev. E* **71**, 061501 (2005).
¹⁷ H. Tanaka, *J. Non-Cryst. Solids* **351**, 678 (2005).
¹⁸ K. Niss, C. Dalle-Ferrer, G. Tarjus, and C. Alba-Simionesco, *J. Phys.: Condens. Matter* **19**, 076102 (2007).
¹⁹ C. De Michele, F. Sciortino, and A. Coniglio, *J. Phys.: Condens. Matter* **16**, L489 (2004).
²⁰ P. Bordat, F. Affouard, M. Descamps, and K. L. Ngai, *Phys. Rev. Lett.* **93**, 105502 (2004).
²¹ V. Molinero, S. Sastry, and C. A. Angell, *Phys. Rev. Lett.* **97**, 075701 (2006).
²² M. Sun, Y. Sun, A. Wang, C. Ma, J. Li, W. Cheng, and F. Liu, *J. Phys.: Condens. Matter* **18**, 10889 (2006).
²³ W. Goetze, *J. Phys.: Condens. Matter* **11**, A1 (1999).
²⁴ W. Kob and H. C. Andersen, *Phys. Rev. E* **51**, 4626 (1995).
²⁵ G. Wahnström, *Phys. Rev. A* **44**, 3752 (1991).
²⁶ S. D. Stoddard and J. Ford, *Phys. Rev. A* **8**, 1504 (1973).
²⁷ R. G. Della Valle, D. Gazzillo, R. Frattini, and G. Pastore, *Phys. Rev. B* **49**, 12625 (1994).
²⁸ B. Bernu, J. P. Hansen, Y. Hiwatari, and G. Pastore, *Phys.*

- Rev. A **36**, 4891 (1987).
- ²⁹ J. P. K. Doye and L. Meyer, Phys. Rev. Lett. **95**, 063401 (2005).
- ³⁰ J. Hernandez-Rojas and D. J. Wales, Phys. Rev. B **68**, 144202 (2003).
- ³¹ G. Tarjus, D. Kivelson, S. Mossa, and C. Alba-Simionesco, J. Chem. Phys. **120**, 6135 (2004).
- ³² A. Mukherjee, S. Bhattacharyya, and B. Bagchi, J. Chem. Phys. **116**, 4577 (2002).
- ³³ T. F. Middleton and D. J. Wales, J. Chem. Phys. **118**, 4583 (2003).
- ³⁴ S. D. Bembenek and B. B. Laird, J. Chem. Phys. **104**, 5199 (1996).
- ³⁵ S. Nosé, J. Phys. Soc. Jap. **70**, 75 (2001).
- ³⁶ M. P. Allen and D. J. Tildesley, *Computer Simulation of Liquids* (Clarendon Press, 1987).
- ³⁷ A. B. Bathia and D. E. Thornton, Phys. Rev. B **2**, 3004 (1970).
- ³⁸ D. Kivelson, G. Tarjus, X. Zhao, and S. A. Kivelson, Phys. Rev. E **53**, 751 (1996).
- ³⁹ S. Sastry, P. G. Debenedetti, and F. H. Stillinger, Nature **393**, 554 (1998).
- ⁴⁰ M. Paluch, A. Patkowski, and E. W. Fischer, Phys. Rev. Lett. **85**, 2140 (2000).
- ⁴¹ R. Casalini and C. M. Roland, Phys. Rev. B **71**, 014210 (2005).
- ⁴² R. Casalini and C. M. Roland, Phys. Rev. E **72**, 031503 (2005).
- ⁴³ A. Reiser and G. Kasper, Europhys. Lett. **76**, 1137 (2006).
- ⁴⁴ K. Niss and C. Alba-Simionesco, Phys. Rev. B **74**, 024205 (2006).
- ⁴⁵ P. Bordat, F. Affouard, M. Descamps, and F. Müller-Plathe, J. Phys.: Condens. Matter **15**, 5397 (2003).
- ⁴⁶ G. F. Voronoi and Z. Reine, Angew. Math. **134**, 198 (1908).
- ⁴⁷ F. H. Stillinger and T. A. Weber, Phys. Rev. A **25**, 983 (1982).
- ⁴⁸ H.-J. Lee, T. Cagin, W. L. Johnson, and W. A. Goddard III, J. Chem. Phys. **119**, 9858 (2003).
- ⁴⁹ C. Hausleitner and J. Hafner, Phys. Rev. B **45**, 115 (1992).
- ⁵⁰ C. Hausleitner and J. Hafner, Phys. Rev. B **45**, 128 (1992).
- ⁵¹ M. Tanemura, Y. Hiwatari, H. Matsuda, T. Ogawa, N. Ogita, and A. Ueda, Prog. Theor. Phys. **58**, 1079 (1977).
- ⁵² J. R. Fernández and P. Harrowell, J. Phys. Chem. **108**, 6850 (2004).
- ⁵³ J. P. K. Doye, A. A. Louis, I.-C. Lin, L. R. Allen, E. G. Noya, A. W. Wilber, H. C. Kok, and R. Lyus, Phys. Chem. Chem. Phys. **9**, 2197 (2007).
- ⁵⁴ C. Donati, S. C. Glotzer, P. H. Poole, S. J. Plimpton, and W. Kob, Phys. Rev. E **60**, 3107 (1999).
- ⁵⁵ J. C. Conrad, P. D. Dhillon, E. R. Weeks, D. R. Reichman, and D. A. Weitz, Phys. Rev. Lett. **97**, 265701 (2006).
- ⁵⁶ W. Kob and H. C. Andersen, Phys. Rev. E **52**, 4134 (1995).
- ⁵⁷ Y. Brumer and D. R. Reichman, Phys. Rev. E **69**, 041202 (2004).
- ⁵⁸ The crossover temperature T_{onset} can be identified by the onset of non-exponential, two-step relaxation in $F_s^\alpha(k^*, t)$.⁵⁶ In constant density simulations, it is also signaled by the sharp decrease of average potential energy of local minima.³⁹ For further interpretation regarding T_{onset} , see Ref.57.
- ⁵⁹ We observed a similar difference in fragility on both smaller ($N = 108$) and larger samples ($N = 6912$) cooled at constant density.
- ⁶⁰ The fraction of icosahedra in local minima also shows, at intermediate temperatures, a shallow minimum, which is more pronounced the more fragile is the mixture, and appears to be a distinct feature of constant pressure simulations.
- ⁶¹ In the models of Hausleitner and Hafner, the interaction parameters become non-additive at large size asymmetry, favoring prismatic geometries. In the case of additive AMLJ- λ mixtures, instead, no sharp structural characterization is apparent at large size asymmetry.